Viscosity effects on Prandtl–Meyer expansion

D.V. Khotyanovsky, P.V. Vashchenkov, A.N. Kudryavtsev and M.S. Ivanov

Institute of Theoretical and Applied Mechanics, Novosibirsk, Russia

Abstract. Effects of viscosity on flow expansion around a convex corner are studied numerically with Navier–Stokes and Direct Simulation Monte-Carlo (DSMC) methods. It is shown that in contrast to the inviscid Prandtl–Meyer flow, angular distributions of temperature and the Mach number are non-monotonous. Viscosity effects cause temperature growth, termination of the Mach number growth, followed by Mach number decrease at higher angles. At higher angles, the Navier–Stokes computations demonstrate rapid increase of the flow temperature and strongly deviate from the DSMC solution. Applicability of the Navier–Stokes approach in the rarefied region is discussed.

Keywords: Flow expansion, Viscosity
PACS: 47.10.ad, 47.15.-x, 47.40.Ki, 47.45.-n

PROBLEM FORMULATION

The classical Prandtl–Meyer solution perfectly describes acceleration of the inviscid supersonic flow in the expansion fan centered at a convex corner. However, at rarefied gas conditions the effects of flow viscosity may become important. More specifically, viscosity can cause flow deflection at larger angles compared to the limiting angle of the Prandtl–Meyer solution. This is important for backflow formation of the nozzle plumes expanding into vacuum. The effects of viscosity on supersonic flow acceleration are also critically important for various microscale devices. This study was also motivated by a fundamental need to define the limits of applicability of the Navier–Stokes equations as the flow density gradually decreases in the expansion region. Therefore, this study was performed with both Navier–Stokes and the DSMC approaches.

We consider here a model problem, which is the supersonic flow over an expansion corner formed by a plane wall (flat plate) suddenly deflecting by a large angle. As a limiting case, where the wall deflection angle reaches 180 °, flow turning around the trailing edge of the infinitely thin flat plate is obtained. Similar model problem was considered by Bird [1] who established a number of important features of such a flow. In particular, he demonstrated that the sonic line, which separated the subsonic part of the flat-plate boundary layer from the supersonic one, terminated at the corner vertex (nozzle lip), so that the subsonic part of the boundary layer was closed.

The flow geometry is shown in Fig. 1. The expansion angle is formed by two walls (Wall 1 and Wall 2) The deflection angle of Wall 2 φ_{w_2} is varied in different simulations. We consider the problem in two formulations. In the first case (designated as "No-BL case" in Fig. 1) the inviscid boundary conditions are imposed on the walls (non-permeability for Navier-Stokes simulations, specular reflection for DSMC). In this case the supersonic oncoming flow is uniform. In the second case ("BL case" in Fig. 1) we impose viscous conditions on Wall 1 (velocity slip and temperature jump conditions Eq. (1) in Navier–Stokes, diffuse reflection in the DSMC simulations). As a result, the supersonic boundary layer is formed on Wall 1 (see Fig. 1). Inviscid boundary conditions are imposed on Wall 2 in both cases.

Using these two separate cases we can distinguish the net effect of the flow viscosity in the expansion flow and the effects of the boundary layer upstream the angle. To exclude any influence of models governing the exchange between translational and internal degrees of freedom of molecules, the computations are performed for a monatomic gas ($\gamma = 5/3$, Argon).

NUMERICAL APPROACH

Navier-Stokes

The two-dimensional Navier-Stokes equations are solved with a shock-capturing MUSCL TVD scheme. The standard van Leer's formula with the *minmod* slope limiter [2] is used for reconstruction of cell-faced variables

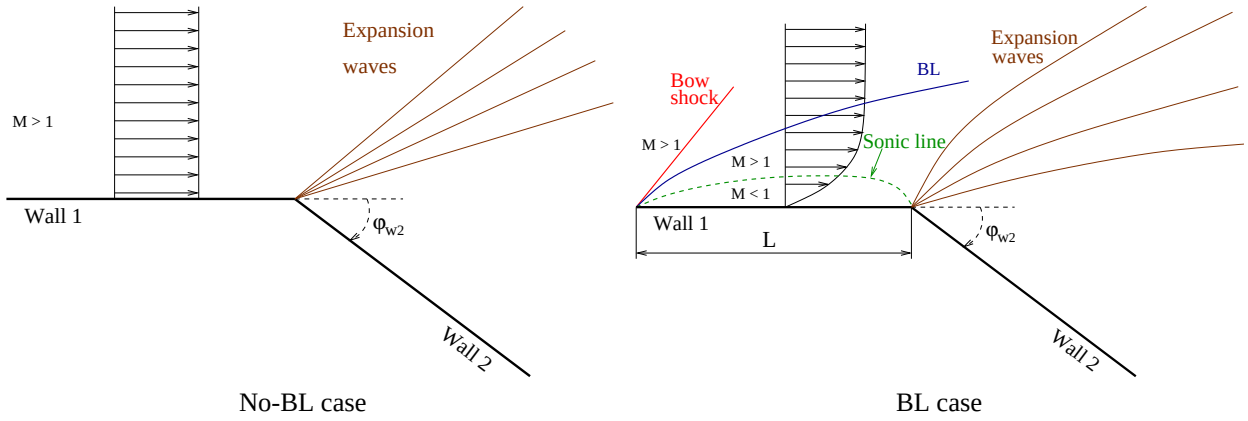

FIGURE 1. Schematic of the flow over an expansion corner without consideration of the boundary layer (left) and with boundary layer effects (right).

from cell-centered ones. The viscous terms are approximated by the central finite differences. HLLEM approximate Riemann solver [3] is employed to calculate the inviscid fluxes. The HLLEM solver is constructed to be robust near low densities and is, therefore, particularly appropriate for simulation of rapidly expanding flows such as in the present paper.

For low-Reynolds-number regimes, the initial rarefaction effects are taken into account by means of imposing velocity slip and temperature jump boundary conditions on solid walls. For this purpose, the slip conditions deduced by Kogan [4] are used:

$$u_\tau = \frac{2-a_u\alpha_u}{\alpha_u}\,\lambda\,\frac{\partial u_\tau}{\partial n}, \qquad T - T_w = \frac{2-a_e\alpha_e}{\alpha_e}\,\frac{\gamma}{(\gamma-1)\mathrm{Pr}}\,\lambda\,\frac{\partial T}{\partial n}, \qquad \lambda = \mu\sqrt{\frac{\pi}{2p\rho}}. \tag{1}$$

Here $a_u = 0.858$ and $a_e = 0.827$ are numerical coefficients derived from an approximate solution of the linearized Boltzmann equation in the Knudsen layer near the solid wall. The accommodation coefficients for momentum α_u and energy α_e are taken equal to unity because no reliable data are available for their values at the present conditions.

DSMC

The DSMC code SMILE [5] developed in Computational Aerodynamics Laboratory, Institute of Theoretical and Applied Mechanics is utilized for kinetic modeling. Intermolecular collisions are computed by the Variable Hard Sphere (VHS) model. The number of collisions is calculated by the majorant frequency method. In the case of a polyatomic gas, the energy redistribution between rotational and translational degrees of freedom is obtained in accordance with the Larsen-Borgnakke model [6] with a constant rotational collision number. Up to $9.6{\cdot}10^6$ molecules are used to simulate the flows under consideration. The computations are performed on a 16-CPU Linux cluster.

RESULTS AND DISCUSSION

No-BL case

The simulations were performed for the following flow parameters: the inflow Mach number $M_\infty = 4.38$ and static flow temperature T_∞=75 K. The unit Reynolds number was varied $\mathrm{Re} = 476, 4760, 47600$ to investigate the effects of flow viscosity. The flow was simulated by the DSMC method and with the Navier–Stokes equations. The Navier–Stokes computations were performed for the expansion corner of $\varphi_w = 37.1^\circ$, which coincides with the maximum Prandtl–Meyer angle $\varphi_{\max}$ for $\gamma = 5/3$ and $M_\infty = 4.38$. Note, the maximum Prandtl–Meyer angle for $\gamma = 5/3$ and $M_\infty = 1$ is 90°. The DSMC computations were performed with $\varphi_w = 37.1^\circ$ and also with $\varphi_w = 180^\circ$, the latter simulates expansion into vacuum around the nozzle lip. The flow was assumed to be two-dimensional.

The typical flowfields obtained are shown in Fig. 2. These computations were performed at the Reynolds number Re = 47600, the wall defelection angle in the DSMC simulation was $\varphi_w = 180^\circ$.

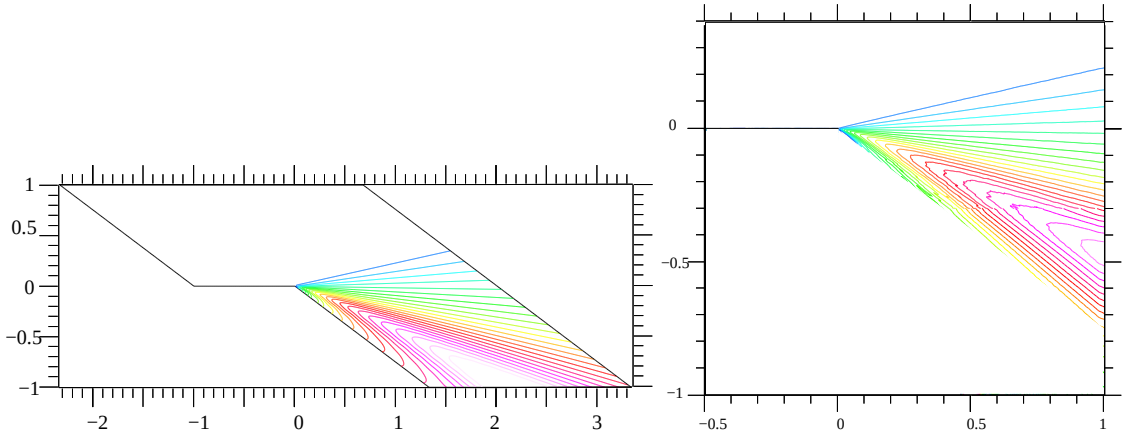

FIGURE 2. Navier–Stokes (left) and DSMC (right) Mach number contours for the flow over an expansion corner with inviscid wall boundary conditions

A close resemblance of two flowfields is worth noting, it holds in spite of the different shape of the computational domains used. Numerical solutions are close to the classical Prandtl–Meyer solution only in some range of polar angles φ (here $\varphi = 0$ corresponds to the axis going along Wall 1, and φ is positive in the clockwise direction). The angular distributions of the flow parameters (non-dimensional density ρ/ρ_∞, Mach number, temperature T/T_∞ and the flow velocity normalized on maximum adiabatic velocity $|\vec{u}|/u_{\max}$) are given in Fig. 3. These distributions were taken along the circle with radius $r/L = 0.4$ centered at the vertex of the expansion corner. For comparison, the inviscid Prandtl–Meyer analytical solution is also plotted in the figures. The DSMC computations in this case were performed for wall deflection $\varphi_w = \varphi_{\max} = 37.1^\circ$ and also for flow expansion into vacuum around the trailing edge, i.e. at $\varphi_w = 180^\circ$. These results are very close to each other, hence only $\varphi_w = \varphi_{\max} = 37.1^\circ$ data are given in the figures. It is evident that the flow viscosity substantially changes the flow around the corner even if the inviscid wall boundary conditions are imposed. This is manifested in termination of growth of the flow Mach number at some polar angle, whose value depends on the Reynolds number, and also in an excessive increase in flow temperature compared to the Prandtl–Meyer solution. These changes become more apparent as the flow Reynolds number decreases. Note, the flow parameters tend to their inviscid limit with increasing Reynolds number. It should be noted that $\varphi_{\max}$ is based on the inviscid theory and does not necessarily hold in this case where the viscous forces produce their effects. Still, in the absence of the boundary layers on the walls that form the expansion corner, the inviscid theory predicts the maximum turning angle quite well. Nevertheless, the density in the Navier–Stokes computations performed with Re = 476 is quite different from zero even for $\varphi = \varphi_{\max}$. The latter, Re = 476, case demonstrates the most prominent differences of the Navier–Stokes results compared to the DSMC computations. These differences are evident in this case from the very beginning of flow expansion. The flow Mach number in Navier–Stokes computations does not grow at all. This is caused by the growth of flow temperature due to the work of viscous forces. Based on this, we can conclude that the Navier–Stokes equations are not applicable to simulation of flow expansion at such a low Reynolds number. For higher Reynolds numbers, i.e., for Re = 4760 and Re = 47600, the Navier–Stokes results are in close agreement with the DSMC computations up to the polar angles $\varphi \approx 5^\circ$ and $\varphi \approx 15^\circ$, respectively.

The applicability of the Navier–Stokes approach can be quantitatively verified using the gradient-length Knudsen number proposed in [7]. If the gradient-length Knudsen number, which is defined here based on local mean free path and density gradient $\mathrm{Kn}_{GL} = \frac{\lambda}{\rho_\infty}|\nabla\rho|$, exceeds 0.05 the flow can no longer be considered continuum. The Kn_{GL} is given in Fig. 4 for the three Reynolds numbers considered here. It is evident that at Re = 476 large part of the computational domain is beyond the limit of the continuum approach.

BL case

To investigate the influence of wall boundary layers, the computations were also performed with the viscous boundary conditions on Wall 1: velocity slip and temperature jump conditions in Navier–Stokes computations, and

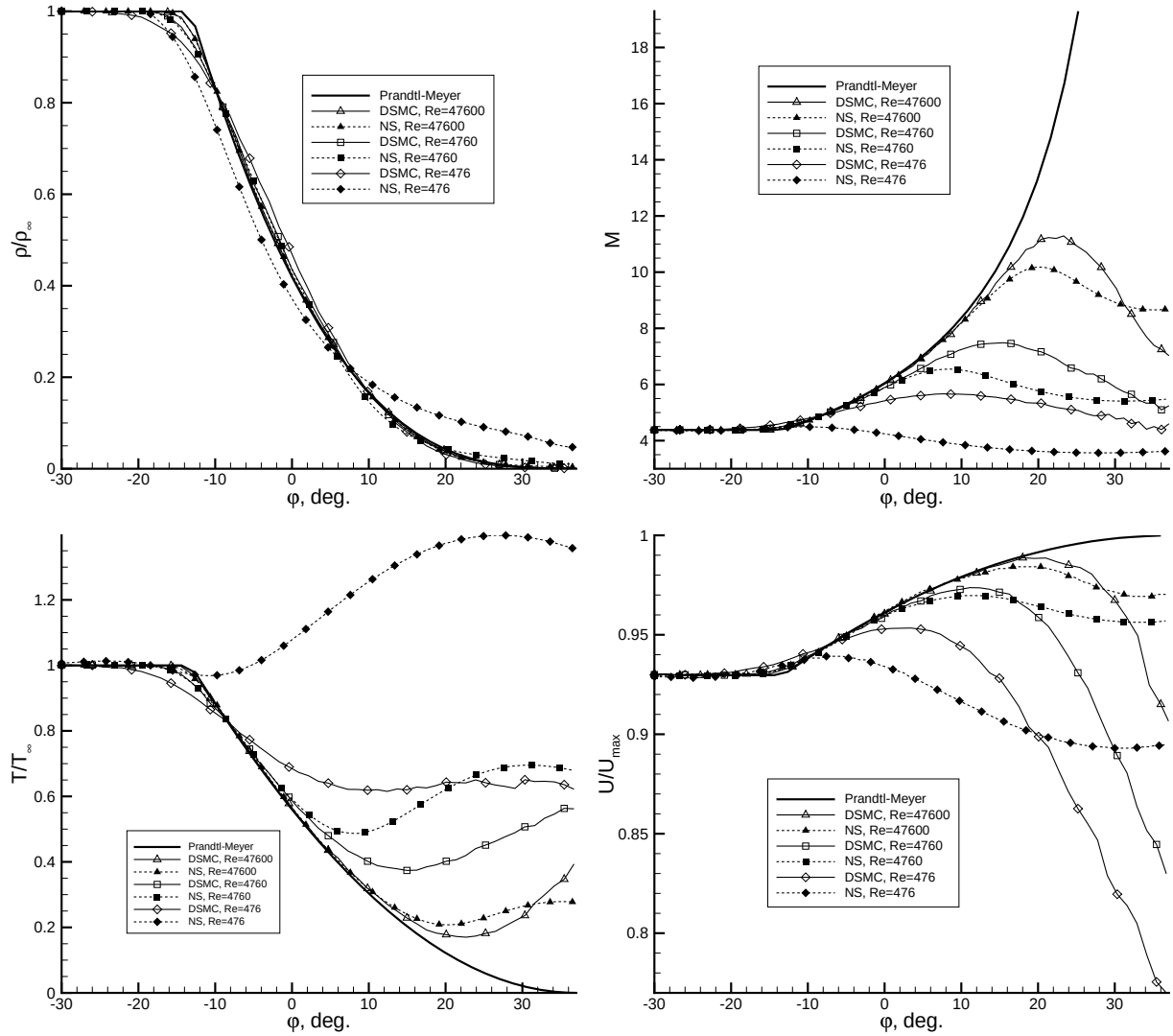

FIGURE 3. Angular distribution of density, Mach number, temperature, and velocity around the expansion corner with inviscid wall boundary conditions

diffuse reflection with the energy accommodation coefficient $\alpha_e = 1$ in DSMC computations. The wall temperature was $T_{w1} = 300$K, and the Reynolds number was $\mathrm{Re} = 4760$. The wall deflection angle in the Navier–Stokes computations was $\varphi_w = 90^\circ$ in this case. On Wall 2, where the flow is extremely rarefied, the inviscid boundary conditions are imposed as in the previous case. Since the flow in the boundary layer upstream of the expansion corner has a much lower Mach number than $\mathrm{M}_\infty = 4.38$, we can expect that the maximum turning angle in this case would be close to $\varphi_{\max} = 90^\circ$ predicted for $\mathrm{M}_\infty = 1$ flow of an inviscid monatomic gas. The DSMC computations were conducted for $\varphi_w = 180^\circ$ turn. The Mach number contours obtained with the Navier–Stokes and the DSMC solvers are given in Fig. 5. The corresponding polar distributions of flow parameters along the circle of radius $r/L = 0.5$ are plotted in Fig. 6.

It is evident that the boundary layer on the wall upstream the expansion corner indeed favors flow deflection at a higher angle. More generally, the boundary layer on the plate favors formation of the backflow. The Mach number around the trailing edge reaches its maximum value near the streamline passing along the outer edge of the boundary layer. The results of Navier-Stokes and DSMC computations agree very well up to the polar angle $\varphi = 10^\circ$ in this case. At higher angles, the Navier-Stokes computations demonstrate a rapid increase in flow temperature, which is probably non-physical. The density becomes close to zero at φ in the range 60-70 degrees. The temperature and,

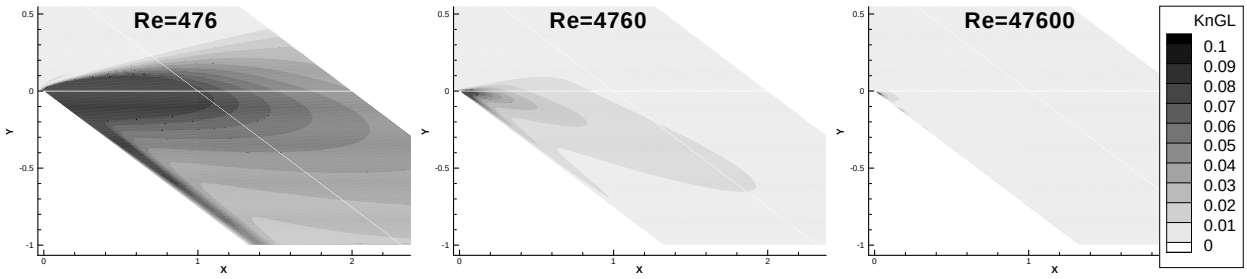

FIGURE 4. Field of gradient length Knudsen number for three Reynolds numbers

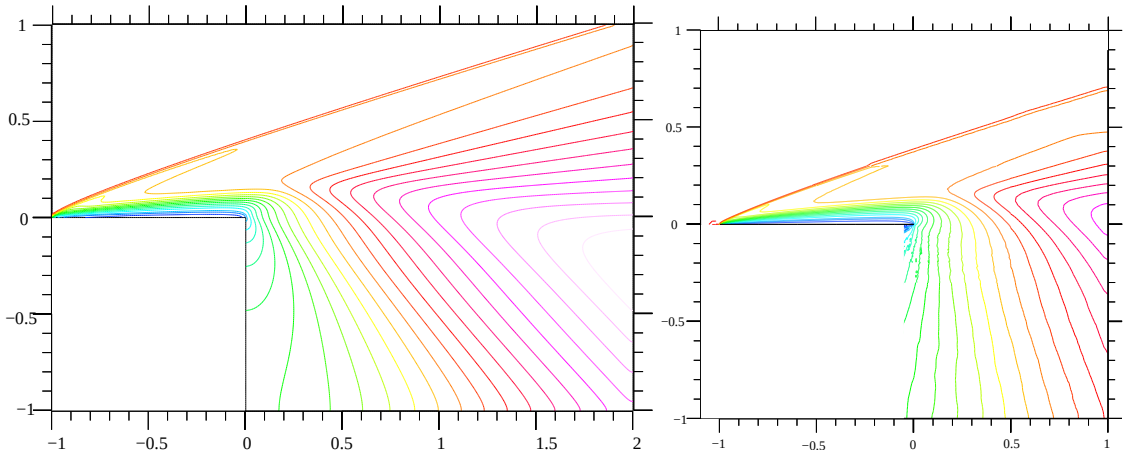

FIGURE 5. Navier–Stokes (left) and DSMC (right) Mach number contours for the flow over an expansion corner with boundary layer on the wall

consequently, the Mach number obtained in the Navier–Stokes computations become apparently different from the DSMC results, starting from $\varphi \approx 0$. What is most important is that the non-physical temperature growth in the Navier–Stokes computations is unlimited (the zero gradient of temperature at $\varphi = 90^\circ$ evident in Fig. 6 is actually the influence of the zero-gradient boundary conditions imposed on the wall located at $\varphi = 90\ ^\circ$). On the contrary, in DSMC computations, the flow temperature tends to its frozen value as the flow is expanded and the inter-molecular collisions become rare.

The excessive non-physical growth of flow temperature observed in the Navier–Stokes computations may cause qualitatively different results in the regions of low-density flow.

CONCLUSIONS

No-BL case. In contrast to the inviscid Prandtl–Meyer flow, angular distributions of temperature and the Mach number are non-monotonous. Viscosity effects cause temperature growth, termination of the Mach number growth, followed by Mach number decrease at higher angles. These effects are most prominent at low Reynolds number. The region of applicability of the Navier–Stokes approach can be identified using the gradient-length Knudsen number as the criterion.

BL case. Boundary layer on the wall favors backflow formation. The Mach number around the trailing edge reaches its maximum near the streamline passing along the outer edge of the boundary layer. The results of Navier–Stokes and DSMC computations agree well up to polar angle 10 deg. in this case. At higher angles, the Navier–Stokes computations demonstrate rapid increase of the flow temperature and strongly deviate from the DSMC solution.

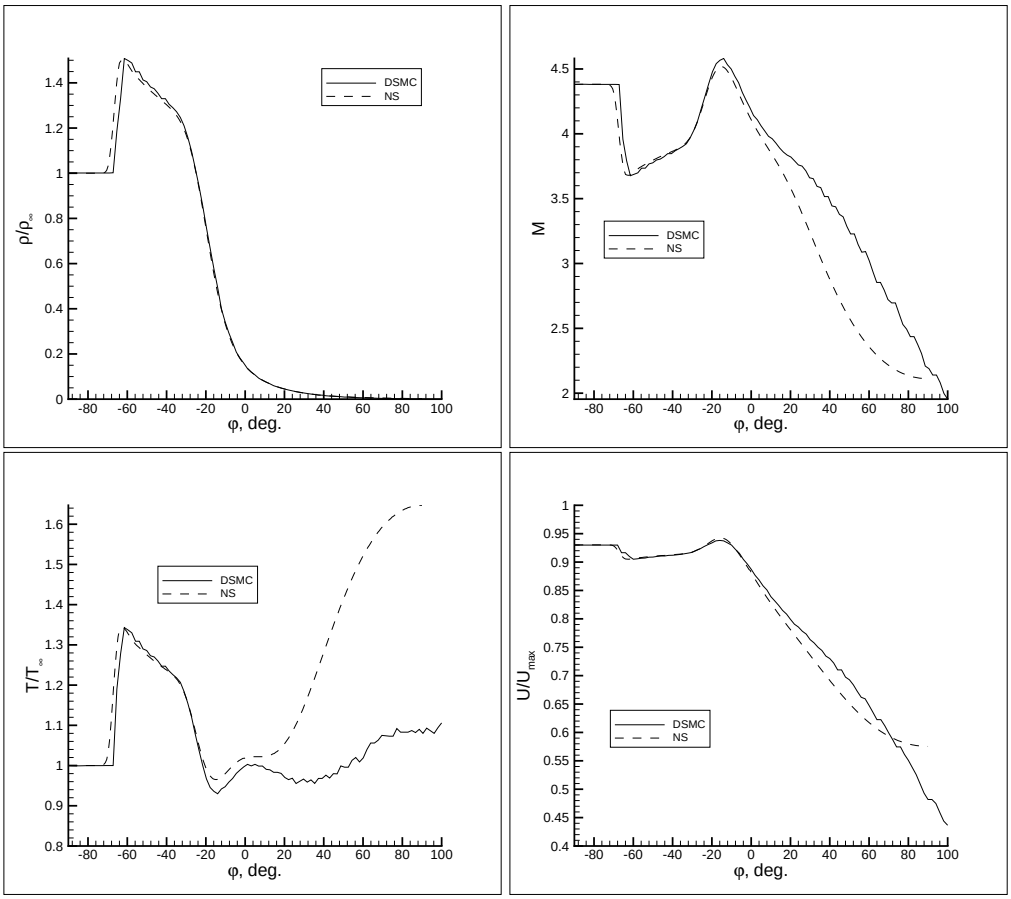

FIGURE 6. Angular distribution of density, Mach number, temperature, and velocity around the expansion corner with viscous wall boundary conditions.

ACKNOWLEDGMENTS

This study was supported by the CNRS and the RFBR in framework of the PICS project, RFBR Ref. No. 06-01-22000.

REFERENCES

1. G. A. Bird, Breakdown of Continuum Flow in Free Jets and Rocket Plumes, *Rarefied Gas Dynamics. Progress in Astronautics and Aeronautics*, **74**, 681–694 (1981)
2. H. C. Yee, A Class of High-Resolution Explicit and Implicit Shock-Capturing Methods, *NASA Technical Memorandum 101088*, 1989.
3. B. Einfeldt, C. D. Munz, P. L. Roe, and B. Sjögreen, *Journal of Computational Physics*, **92(2)**, 273–295 (1991).
4. M. N.Kogan, *Rarefied Gas Dynamics*, Plenum Press, New York, 1969.
5. M. S. Ivanov, G. N. Markelov, S. F. Gimelshein, *AIAA Paper 98-2669*, 1998.
6. C. Borgnakke, and P. S. Larsen, *Journal of Computational Physics*, **18(3)**, 405–420 (1975).
7. I. D. Boyd, G. Chen, G. V. Candler, *Physics of Fluids*, **7**, 210-219 (1995).